**Article:**
Yu, K, Zhang, H, Tangparitkul, S et al. (3 more authors) (2022) Interfacial behavior of core–shell composite nanoparticles under compression and shear: Influence of polymer shell thickness. Journal of Colloid and Interface Science, 613. pp. 827-835. ISSN 1095-7103

https://doi.org/10.1016/j.jcis.2022.01.069

# Interfacial behavior of core-shell composite nanoparticles under compression and shear: influence of polymer shell thickness

Kai Yu[a*], Huagui Zhang[b], Suparit Tangparitkul[c], Jiatong Jiang[d], Chris Hodges[d] and David Harbottle[d*]

[a] School of Energy and Power Engineering, Jiangsu University, Zhenjiang, China, 212013

[b] College of Chemistry and Materials Science, Fujian Key Laboratory of Polymer Science, Fujian Normal University, Fuzhou 350007, China

[c] Department of Mining and Petroleum Engineering, Faculty of Engineering, Chiang Mai University, Chiang Mai 50200, Thailand

[d] School of Chemical and Process Engineering, University of Leeds, UK

## ABSTRACT

**Hypothesis:** The mobility of core-shell nanoparticles partitioned at an air-water interface is strongly governed by the compliance of the polymer shell.

**Experiments:** The compressional, relaxation and shear responses of two polymer-coated silica nanoparticles (CPs) were studied using a Langmuir trough and needle interfacial shear rheometer, and the corresponding structures of the particle-laden interfaces were visualized using Brewster angle and scanning electron microscopy.

**Findings:** The mobility of CPs partitioned at an air-water interface correlates to the polymer MW. In compression, the CPs40-laden interface (silica nanoparticles coated with 40 kDa PVP) showed distinct gas-liquid-solid phase transitions and when the surface pressure was reduced, the compressed particle-laden interface relaxed to its original state. The compressed-state of the CPs8-

laden interface did not relax, and wrinkles in the particle-laden film that had formed in compression remained due to greater adhesion between the compressed particles. The increased mobility of the CPs40-laden interface translated to lower surface shear moduli, with the viscoelastic moduli an order of magnitude or more lower in the CPs40-laden interface than the CPs8-laden interface. Ultimately this contributed to changing the stability of particle-stabilized foams, with less mobile interfaces providing improved foam stability.

**Keywords:** Polymer-coated particles; Interfacial shear rheology; Particle-laden interfaces

## 1. INTRODUCTION

Nanoparticles self-assembly at liquid-air interfaces is of great importance and widely found in optoelectronic metamaterials,[1] colloidal lithography[2] and stabilizing foams.[3-6] The orientation of particles at the interface often governs material performance, with the positioning of particles at an interface influenced by electrostatic forces, monopolar and dipolar interactions, and wetting forces.[7] The latter depends on the wetting characteristics of the nanoparticles in liquids that are often of contrasting polarity.[8] Routes to enhance the partitioning of nanoparticles at liquid-air interfaces include surface modification using small molecules[9] and chemical grafting or adsorption of higher molecular weight polymers to enhance the hydrophobicity of nanoparticles.[10, 11] In the latter, the polymer shell encapsulates the nanoparticle to form a steric barrier which can be modulated by changing the polymer molecular weight, chemistry and architecture, as well as the polymer solvation in the liquid phase.[12, 13] When highly solvated, polymer chains tend to spread at the liquid-air interface, with the polymer extension balanced by the internal elasticity of the polymer.[14] The opposite occurs in a poor solvent, with the polymer chains collapsing to form globules on the particle surface.[15, 16] Such control provides a route to modulate the contribution of steric forces relative to other forces such as electrostatic, monopolar and dipolar interactions.[7]

The self-assembly of core-shell particles at liquid-liquid interfaces can be studied using Langmuir troughs.[7] When studying the self-assembly of $SiO_2$@PNiPAm core-shell particles partitioned at

an air-water interface, small changes in the molecular weight of grafted PNiPAm increased the polymer shell thickness from 70 to 130 nm, but led to significant changes to the centre-to-centre particle-particle separation distance, increasing from 400 to 1280 nm and up to 8 times the size of the particle diameter.[16] Two phases, corresponding to shell-shell and particle core-particle core contacts were observed when the particle-laden film was compressed, with the shell-shell contacts mechanically failing before particle core-particle core contacts prevailed.[8] The critical surface pressure to induce those phase transitions depended on the polymer shell thickness,[16] with the compliance of the shell more pronounced for thick polymer layers, leading to better defect compensation in the particle-laden film.[2] In compression, the resistance to particle reorganization can be modulated by the polymer shell thickness, with thin (relative to the particle radius) polymer layers exhibiting low compressibility.[6]

Compression of the particle-laden interface leads to higher surface pressures as the particle network begins to resist the normal applied load. In compression, the interfacial shear rheology of the particle-laden film will also change,[7] but this less commonly discussed as few techniques provide the capability of measuring the interfacial shear rheology of a compressed film. The interfacial stress rheometer (ISR) is one such technique that has been used by several groups and relies on positioning a small magnetic rod at the air-liquid interface, which is then oscillated by a magnetic field gradient generated by a pair of Helmholtz coils surrounding the Langmuir trough.[17] To date, the technique has been used to study the interfacial shear rheology of polymers, polymer-surfactant complexes, proteins, lipids, solid particles and core-shell particles.[7, 17-21] For particle-laden interfaces, the surface shear moduli has been shown to undergo a liquid-to-solid transition with increasing surface pressure,[7, 22] where the magnitude of the interfacial viscoelastic moduli was found to be determined locally by the degree of restricted particle motion that is dictated by both the particle-particle interaction strength and severity of caging caused by the local microstructure.[23]

Researchers have synthesized core-shell composite particles via chemical grafting methods[2, 8, 13, 24] but less is known about the interfacial behavior of core-shell nanoparticles formed via physical adsorption. The physical adsorption method is attractive as it can be easily scaled,

however, the polymer binds to the nanoparticle via multiple contacts to form an expanded polymer shell typically of loops and tails orientation, therefore the arrangement and polymer coverage may not be uniform.[25]

Recently, Poly(vinylpyrrolidone) (PVP)-coated silica nanoparticles (CPs) have been prepared via the physical adsorption method,[15, 26] and their partitioning at an air-water interface revealed a dominance of the PVP-PVP interaction to modulate the compressibility of CPs-laden interfaces.[15] The effect of PVP molecular weight was influential in modifying the mechanics of the particle-particle contacts.[25] Low molecular weight PVP (8 kDa) formed a flat, thin film on planar silica surface (layer thickness of ~0.7 nm, surface excess of ~0.8 mg/m$^2$), and was characterized as being rigid and weakly solvated. For higher molecular weight PVP (40 kDa), the adsorbed film was thicker, more solvated and exhibited viscoelastic properties (layer thickness of ~1.8 nm, surface excess of ~1.0 mg/m$^2$).[25] Such changes in the polymer film viscoelasticity were able to reduce the contact friction between surfaces by a factor of ~2.[25]

The current study explored the potential of using different molecular weight PVPs to control the response of particle-laden interfaces subjected to changing surface pressures. Using low (8 kDa) and intermediate (40 kDa) molecular weight PVPs, the compressibility, interfacial structure and interfacial shear rheology were compared for the two particle types and as a function of surface pressure. The fundamental link between structure of the particle network and interfacial shear rheology was used to describe the observed differences in foam stability.

## 2. MATERIALS AND METHODS

**2.1 Materials.** Ludox AS40 silica nanoparticles were supplied by Sigma-Aldrich (UK) as a 40 wt% aqueous suspension. Polyvinylpyrrolidone (molecular weights of 8 kDa and 40 kDa) was supplied by Alfa Aesar (UK) and used without further purification. Milli-Q water with a resistivity of 18.2 MΩ.cm was used throughout the study and sodium sulphate (99+%. A.C.S. R, Sigma Aldrich, UK) was used to adjust the electrolyte concentration. All chemicals were used without further purification.

**2.2 Preparation of PVP-coated silica nanoparticles (CPs).** Two types of CPs were prepared using a one-step physical adsorption method, with further details of this method provided in the Supporting Information and reference.[15] CPs8 and CPs40 is used throughout as an abbreviation for the silica nanoparticles coated with 8 and 40 kDa PVP, respectively. The successful preparation of the core-shell structure of the two CPs was verified by transmission electron microscopy (FEI Tecnai TF20, UK) as shown in Fig. 1b, and thermo-gravimetric analysis (Q-500 TA Instruments, USA) as shown in Fig. S1.

**2.3 Characterization of particle-laden interfaces.** *2.3.1 Π-A Isotherms.* Surface pressure–area ($\Pi$ – A) isotherms of CPs-laden interfaces were studied using an air-liquid Langmuir trough (Biolin Scientific, Sweden), with a maximum trough area of 280 $cm^2$. The CPs were first dispersed in a spreading solvent (water:isopropanol alcohol = 1:1 vol. ratio) to a concentration of 0.5 wt%. The liquid phase was 5 mM $Na_2SO_4$, and 80 µL of the 0.5 wt% particle suspension was deposited carefully and evenly at the air-aqueous interface using an 50 µL Hamilton syringe with a 22s gauge blunt-end needle. The deposited CPs film was left undisturbed for 30 min to evaporate the spreading solvent, before using both barriers of the Langmuir trough to compress the interfacial film at a constant rate of 50 $cm^2$/min.

Multiple compressions were carried out to study the compressional hysteresis of the interfacial films. After the first compression, the two barriers were withdrawn at 50 $cm^2$/min to 280 $cm^2$ and then immediately the interfacial film was compressed again at the same rate for a second time. All measurements were repeated in triplicate with good reproducibility observed. Further details on the trough cleaning procedure, experimental setup and method can be found in Yu et al..[15]

*2.3.2 CPs-laden interface structure.* The structure of the CPs-laden interface was measured at different surface pressures using a Brewster Angle Microscope (BAM, Model EP3, Accurion GmbH, Germany) combined with the Langmuir trough.[27, 28] Before particle deposition, the calibrated Brewster angle of the clean air-aqueous interface (5 mM $Na_2SO_4$) was 53.23°. Following

calibration, 80 μL of 0.5 wt% CPs suspension was deposited at the air-aqueous interface. After waiting for 30 min, the CPs-laden interface was compressed to surface pressures of 0.5, 1, 2, and 3 mN/m. The compressed CPs-laden interface was then allowed to relax for 1 min before imaging by BAM at constant surface pressure, with the surface pressure maintained by initializing the 'surface pressure control mode' of the Langmuir trough. More details on the BAM setup and experimental methods can be found in Yu et al..[7]

*2.3.3 Interfacial stress rheology (ISR).* The shear rheology of the CPs-laden interfaces were studied using an Interfacial Stress Rheometer (ISR400, Biolin Scientific), combined with a Langmuir trough (Biolin Scientific),[7, 19] see Fig. S2 for more details. Briefly, the magnetic needle oscillates sinusoidally (induced by the Helmholtz coils) at an amplitude ratio, AR, defined as the ratio of the amplitude of the rod displacement (strain, $\gamma$) to the forcing amplitude (stress, $\sigma$), with the strain and stress offset being the phase difference ($\delta$). The dynamic surface modulus, $G^*$, which is given by $G^*(\omega) = G'(\omega) + iG''(\omega)$, can be determined directly from AR and $\delta$:

$$G^*(\omega) = \frac{1}{AR} e^{i\delta} = G'(\omega) + iG''(\omega) \quad (1)$$

where $G'$ and $G''$describe the storage and loss moduli of the interfacial film, respectively.

An air-aqueous interface was formed by gently pouring 400 mL of 5 mM $Na_2SO_4$ into the Langmuir trough. Then the magnetic needle was positioned at the air-aqueous interface within a glass channel. The mobility of the magnetic needle was calibrated on a particle-free interface such that the combined contribution from the sub-phase and needle inertia could be subtracted from the measured response when oscillated in the presence of CPs. 80 μL of 0.5 wt% particle suspension was then deposited drop-wise at the air-aqueous interface. After waiting for 30 min, the particle-laden interface was compressed to surface pressures of 0.5, 1, 2, 3, and 4 mN/m, and the interfacial shear rheology measured at those pressures. For all CPs-laden interfaces, the dimensionless Boussinesq number (*Bo*) was $\geq$ 20, and thus the sub-phase contribution to the measured

viscoelasticity was considered negligible. Hence, all experimental data was presented without the need of further processing.[29] [7]

For all CPs-laden interfaces, a dynamic strain sweep (amplitude sweep) was first conducted at a fixed frequency of 0.5 Hz (3.14 rad/s) to determine the linear viscoelastic region. To probe the time-dependent response of the CPs-laden interfaces, frequency sweep measurements were conducted between 0.1 Hz (0.63 rad/s) and 5 Hz (31.40 rad/s). All interfacial rheology tests were repeated in triplicate and showed good repeatability. More details on the ISR setup and experimental method can be found in Yu et al..[7]

**2.4 Foam Studies.** Foams were prepared by adding 10 mL of 1 wt% CPs (either CPs8 or CPs40) in 5 mM $Na_2SO_4$ to a 40 mL glass vial, and then tip sonicated for 10 s (120 W, with ice bath cooling, VCX500) to generate the foams. Foamability and foam stability were measured by analysing images of the foams taken immediately after foaming and then at regular time intervals up to 150 min. The sizes of individual bubbles in the foam were measured using an optical microscope (Olympus BX51). After foaming, the foam was immediately extracted from the glass vial by capillary action into a flat-edged capillary tube ($0.5 \times 5$ mm$^2$). The capillary tube was sealed at both ends using Parafilm® tape and left undisturbed in the microscope for imaging.

## 3. RESULTS AND DISCUSSION

**3.1 Characterization of CPs.** When compared to the silica nanoparticles, the CPs particles showed a core-shell structure (Fig. 1a, TEM images), with the average thickness of the polymer shell determined (using ImageJ) to be ~1.4 nm and ~2.9 nm for the CPs8 and CPs40 particles, respectively. The difference in polymer shell thickness was also qualitatively verified by the haziness of the CPs40 particles (Fig. 1a), which occurs due to the thicker polymer film of the higher molecular weight polymer. However, it should be noted that those particles were dried on a TEM stub, and therefore, the hydrated polymer shell thickness will be greater. The PVP surface excess ($\Gamma$) on silica was measured by TGA and found to be ~0.70 and ~0.88 mg/m$^2$ for CPs8 and

CPs40, see Fig. S1 and Table S1. Those values are in good agreement with the PVP surface excess measured on silica using the quartz crystal microbalance technique, which was also used to confirm the long-time stability of the adsorbed PVP film and its resistance to washing.[25] From the TEM images it appeared the PVP coating was almost uniform on the silica nanoparticles, which likely corroborates the DLS data where the mean hydrodynamic diameters ($D_h$) of the silica nanoparticles, CPs8 and CPs40 in Milli-Q water were ~34 nm, ~40 nm, and ~52 nm, with a PDI of ~0.14 (for all samples), indicating that the average thickness of the hydrated PVP shell for CPs8 and CPs40 was ~3 nm and ~9 nm (Table S1).

When dispersed in 5 mM $Na_2SO_4$, the $D_h$ of the three particle types, silica nanoparticles, CPs8 and CPs40 were ~34 nm, ~39 nm, and ~50 nm, respectively. The decrease in $D_h$ from Milli-Q water is due to the changing polymer conformation, with the polymer collapsing onto the particle surface as the polymer solvency is reduced in the divalent electrolyte solution, which was also confirmed in our previous study.[15] The electrophoretic mobility of the composite particles were measured using a ZetaSizer Nano ZS (Malvern Instruments, UK). When dispersed in 5 mM $Na_2SO_4$, the electrophoretic mobilities of CPs8 and CPs40 were relatively high (~−2.3 μm·cm/(Vs)), although slightly lower than those measured in Milli-Q water (~−2.5 μm·cm/(Vs)). Based on the DLS and electrophoretic mobility data, the CPs were considered to be non-interacting and well-dispersed in 5 mM $Na_2SO_4$.

**3.2 Π – A isotherms and interfacial structure.** *Π-A* isotherms and the normalized surface elasticities (relative to the trough area at film collapse ($A_c$)) are shown in Fig. 1b for CPs8 and CPs40 particle-laden films (the raw data is provided in Fig. S3). While the silica particles were too hydrophilic to partition at the air-water interface, their attachment could be improved by the PVP coating. With the polymer less solvated in $Na_2SO_4$, the affinity of the CPs to the air-liquid interface was enhanced relative to Milli-Q water.[15] Although the polymer surface excess ($\Gamma$) on silica was similar for both 8 and 40 kDa PVP (Table S1), the thickness of the solvated 40 kDa PVP shell was ~3 times that of the 8 kDa PVP shell (Table S1). However, this difference maybe be further increased when particles are partitioned at the air-liquid interface. It has been shown that polymers

spread at the air-liquid interface, with the limit of spreading inhibited by the internal elasticity of the polymer. The relative change in the apparent size of PNIPAM hydrogels at an interface compared to bulk has been reported to be ~1.6-1.8.[2] Such spreading leads to an increase in the area occupied by the particle, as schematically shown in Fig. 1c.[2, 14] Assuming an equal number of particles were retained at the air-liquid interface, the thicker, more expanded polymer film would contribute to occupying more surface area, thus generating a higher surface pressure at an equivalent trough area, and shown in Fig. S3.

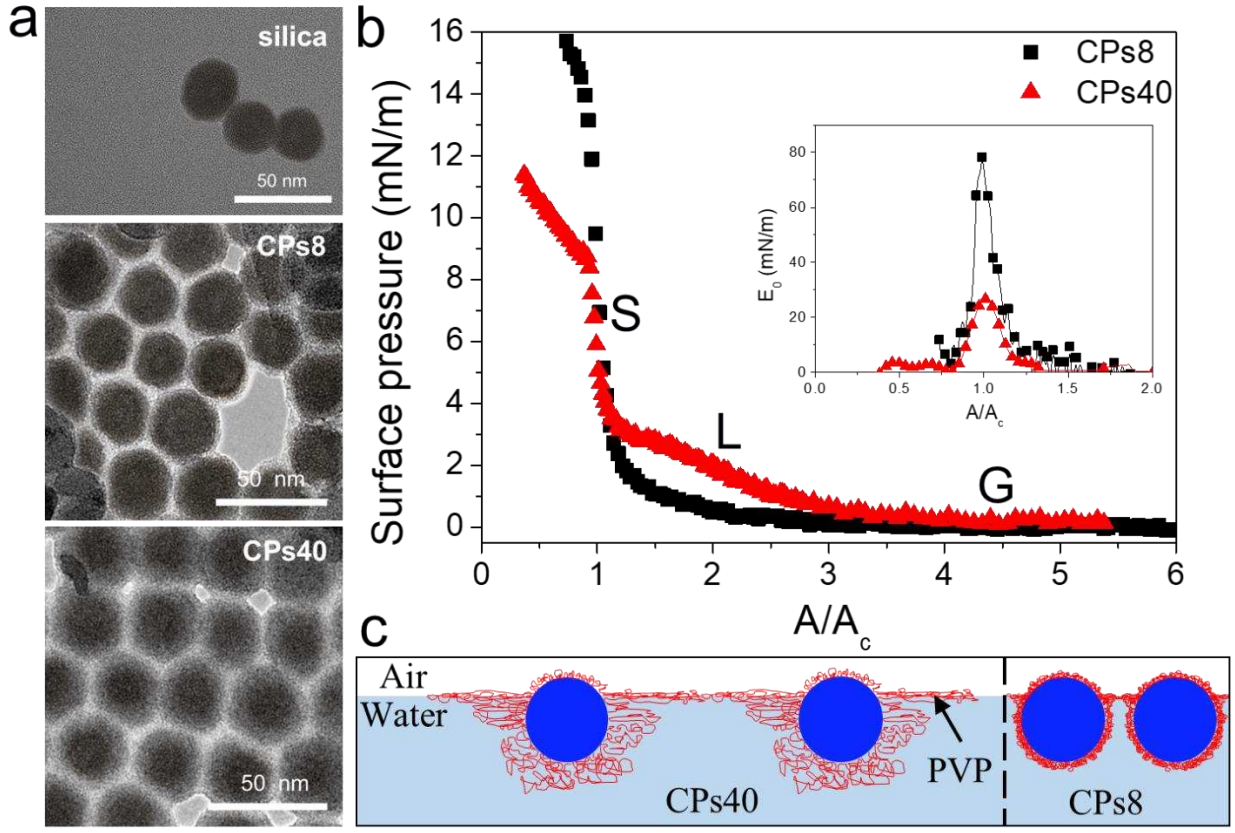


**Figure 1.** a) TEM images of the silica, CPs8 and CPs40 nanoparticles, with a clear core-shell structure being observed for the two CPs samples. b) $\Pi - A$ isotherms and surface elasticities (inset) that are normalized by the trough area at film collapse. $A$ refers to the trough area and $A_c$ is the trough area at film collapse, which for CPs8 and CPs40-laden interfaces was ~25.6 cm$^2$ and ~52.8 cm$^2$ respectively. The raw data is provided in Fig. S3. c) Schematic showing the likely

partitioning of CPs8 and CPs40 at the air-water interface. The CPs40 polymer shell is thicker than the CPs8 polymer shell and could expand further at the air-water interface.

In compression, the CPs40-laden interface exhibited distinct gas (G), liquid (L) and solid (S) phase behavior, with the L-S phase transition observed at ~3 mN/m before the film collapsed (buckled) at ~8 mN/m. Previously, the interaction between PVP-PVP had been measured to be purely repulsive when the electrolyte concentration was < 0.1 M $Na_2SO_4$.[15] At the test conditions, the Debye length is ~3 nm in 5 mM $Na_2SO_4$, which is less than the thickness of the solvated 40 kDa PVP film (~8 nm), suggesting the particle-particle interaction is strongly influenced by the steric barrier. When compressed, the steric barrier compensates the applied normal load to resist hard surface contact (particle core–particle core contacts), As such, the particle-particle contacts are more lubricated which enables the particles to reorganize more easily, thus leading to a gradual increase in surface pressure, as shown by the L-phase up to ~3 mN/m. However, in the S-phase ($\Pi$ > 3 mN/m) the polymer shell of the nanoparticles will be significantly compressed, and thus in-plane particle rearrangement becomes restricted, as seen by a rapid increase in surface pressure (at an increasing rate of $0.36\times10^4$ mN/m$^3$) up to the film collapse at ~8 mN/m.

For the CPs8-laden interface, the L-phase was less distinct. At the test conditions, the thickness of the 8 kDa PVP film (~2.5 nm) is comparable to the Debye length (~3 nm). The L-S phase transition occurred at ~1 mN/m, with a much steeper rise in surface pressure in the S-phase (at an increasing rate of $1.52\times10^4$ mN/m$^3$) compared to the CPs40-laden interface. From the compression response, the CPs8 particles behaved more like hard-spheres, providing less resistance to compensate the applied normal load, and attaining the S-phase response at a lower critical surface pressure, $\Pi$ ~1 mN/m. The particle-film collapse pressure was ~15 mN/m, almost double that of the CPs40-laden interface. A similar trend in film collapse pressure has been observed for microgels particles,[2, 30] where the collapse pressure decreases with increasing particle softness (e.g. by reducing the cross-link density of the microgels). The thicker PVP shell increases the “softness” of CPs to reduce the apparent stress between contacting particles. However, once in-plane particle rearrangement becomes prohibitive, the increasing compressional stress is relieved by expelling particles from the monolayer network, as the compressional stress exceeds the contact stress.[31]

The lower surface pressure at this condition confirms it is easier to displace CPs40 than CPs8 from the particle-laden film, and this difference is likely attributed to a higher lubricity between particle contacts of CPs40.[25]

The surface elasticity corresponds to the stiffness of the particle-laden film, which was calculated by, $E_0 = -\frac{d\Pi}{dlnA}$ (where $A$ is the trough area and $\Pi$ the surface pressure), for both CPs8 and CPs40-laden interfaces under increasing compression, see inset Fig. 1b. The raw data is shown in Fig. S3. At the critical condition of film collapse, $A/A_c = 1$, the maximum surface elasticity of the CPs8-laden interface was ~80 mN/m and almost 3 times greater than the CPs40-laden interface (~28 mN/m), confirming the greater rigidity of the particle-laden film at the critical collapse pressure.

BAM was used to image the CPs-laden interfaces at $\Pi \leq 3$ mN/m (Fig. 2a). For CPs40 at $\Pi = 0.5$ mN/m, the BAM image appeared featureless and uniformly dark gray (measured gray-scale color intensity ~25), likely due to good dispersion of the CPs40 particles at the air-water interface which result from the strong steric barrier. Under compression ($\Pi$ = 1, 2, 3 mN/m), the BAM images become increasingly brighter due to a decreasing interparticle separation distance and increasing particle packing density. For all measurements, the apparent change in particle packing density can be pseudo-quantitatively assessed by the value of the gray-scale color intensity (Fig. 2b).

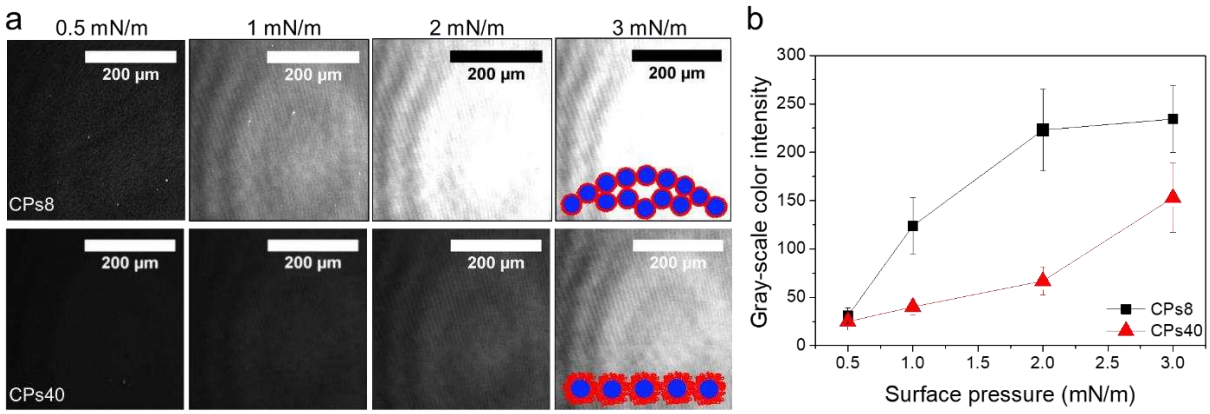


**Figure 2.** a) BAM images of CPs8 and CPs40-laden interfaces at increasing surface pressures. The inset schematics are included to show the hypothetical structure (side view) of the two CPs-laden interfaces under compression. In the S-phase (CPs8, $\Pi \geq 1$ mN/m), the high brightness of the images likely indicates bending and/or multi-layering of the particle-laden film. b) Mean gray-scale color intensity values corresponding to the images in (a).

At low surface pressure ($\Pi$ = 0.5 mN/m) the mean gray-scale color intensity values were similar for both particle-laden interfaces, but the gray-scale color intensities rapidly deviated as the surface pressure increased. The CPs8-laden interface appeared much brighter at higher surface pressures ($\Pi$ = 1, 2, 3 mN/m). The dullness of the CPs40-laden interface was further evidence that the particle-laden interface remained in the L-phase up to 3 mN/m, with the strong steric barrier of the PVP coating resisting close confinement of particle cores (inset schematic in Fig. 2a). This contrasts the CPs8-laden interface that transitioned to the S-phase at $\Pi$ = 1 mN/m, with the BAM images at higher surface pressures representing a condition of maximum particle-particle compression, and the increased image brightness is likely attributed to gradual bending of the particle-laden interface and/or particle displacement to form stacked particle layers.[15]

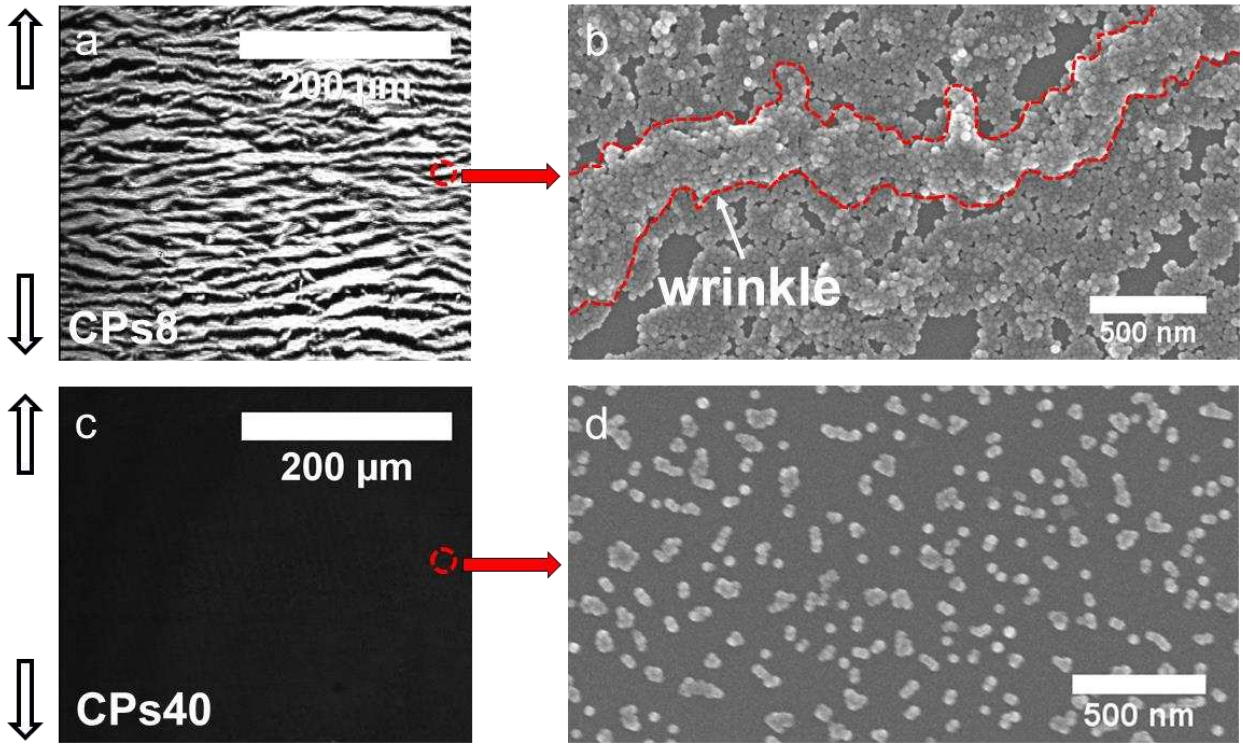


**Figure 3.** BAM images of relaxed CPs-laden interfaces at $\Pi = 0.5$ mN/m. The CPs-laden interfaces were first compressed to $\Pi = 3$ mN/m before increasing the surface area by moving the barriers in the direction of the arrows (a and c). The relaxed CPs-laden interfaces were transferred onto mica substrates using the Langmuir-Blodgett (LB) deposition technique and the micron-scale structure observed by SEM imaging (CPs8 – b and CPs40 – d).

Relaxed structures of compressed CPs-laden interfaces are shown in Fig. 3. The particle-laden interfaces were first compressed to $\Pi = 3$ mN/m before expanding the surface area to lower the surface pressure to 0.5 mN/m. It is worth noting that $\Pi = 3$ mN/m corresponds to the S-phase for CPs8 and the L-S phase transition for CPs40, which along with the differences in PVP layer-thickness, likely contribute to the contrasting 'relaxed' states of the CPs-laden interfaces. Based on previous analysis of the BAM images, the CPs40-laden interface appeared almost featureless with a mean gray-scale color intensity of 25 ± 4 (Fig. 3c), analogous to the BAM image at $\Pi = 0.5$ mN/m prior to first compression (Fig. 2a). Moreover, the CPs8-laden interface showed bands of light and dark regions (Fig. 3a), indicating the compressed particle layer undergoes negligible relaxation. High resolution SEM images were obtained by transferring the interfacial films onto

mica substrates using the Langmuir-Blodgett (LB) deposition technique. As shown in Figs. 3b and d, the SEM images complement the BAM images, showing the CPs40 particles to be well dispersed (small aggregates of a few particles, Fig. 3d), and the CPs8 particles strongly clustered, both in-plane (2D) and out-of-plane (3D) of the air-water interface (Fig. 3b). When compressed in the S-phase, particle-laden interfaces are known to wrinkle and buckle when the critical compressive strain is exceeded. The light bands in the BAM image are unrelaxed wrinkles (as highlighted by the dashed red line in Fig. 3b). While it is difficult to verify, separation of unrelaxed wrinkles will occur between weak particle-particle contacts, and given how wrinkles form, those weaker contacts are likely to occur in the trough between two wrinkles, i.e. in the 2D-plane of the interfacial film. The ability for a wrinkle to relax will be hindered by the number of particle-particle contacts and particle confinement, as well as any dehydration of the polymer-particle network that can occur when a wrinkle undergoes vertical displacement from the water-air interface.

Using atomic force microscopy with colloidal probe, adhesion forces between 8 kDa and 40 kDa PVP films were measured in Milli-Q water, see Fig. S4. The PVP films were compressed to a normal force of ~17.5 nN and held in contact for up to 300 s. At short contact times the difference between the two polymer systems was found to be negligible, but for extended contact times the adhesion force of 8 kDa PVP exceeded that of 40 kDa PVP. While the PVP films remained hydrated, the stronger adhesion force between 8 kDa PVP at longer contact times likely contributed in-part to the irreversibility of the compressed particle network. The molecular weight dependence on adhesion force has been considered in detail by others[32] and discussed in the context of relaxation times, with higher molecular weight polymers exhibiting longer reptation times. The greater adhesion for 8 kDa PVP may also result from polymer chains bridging the two surfaces, and the possibility of vdW attraction if the two surfaces are pushed into hard contact. Furthermore, our previous study found that partial dehydration of two interacting polymer films (PVP) showed an approximate doubling in the lateral force,[25] and thus significant hindrance to particle mobility will occur.

The contrasting relaxation responses of the two CPs-laden interfaces is also seen through consecutive compressions of the interfacial film. Two compressional isotherms up to $\Pi = 4$ mN/m

(such that both films were compressed into the S-phase region) are compared in Fig. 4. For the CPs40-laden interface, the two compressional isotherms remain almost consistent with surface area, with the second isotherm approximately 0.1 mN/m lower than the first isotherm. Although not directly evidenced, the small difference between the first and second isotherms may indicate some particles were displaced from the air-water interface and/or full relaxation of the particle-laden interface had not been achieved (see Fig. 3d which shows small clusters of CPs40). For the CPs8-laden interface that showed negligible interfacial film relaxation (Figs. 3a and b), the two compressional isotherms deviated substantially at low surface areas. To attain an equivalent surface pressure of 0.5 mN/m, the surface area of the first and second compression was 54 $cm^2$ and 38 $cm^2$. The lower surface area in the second compression would be consistent with the irreversible densification of the particle network, hence greater compression (lower surface area) is needed to reform a contiguous particle network.

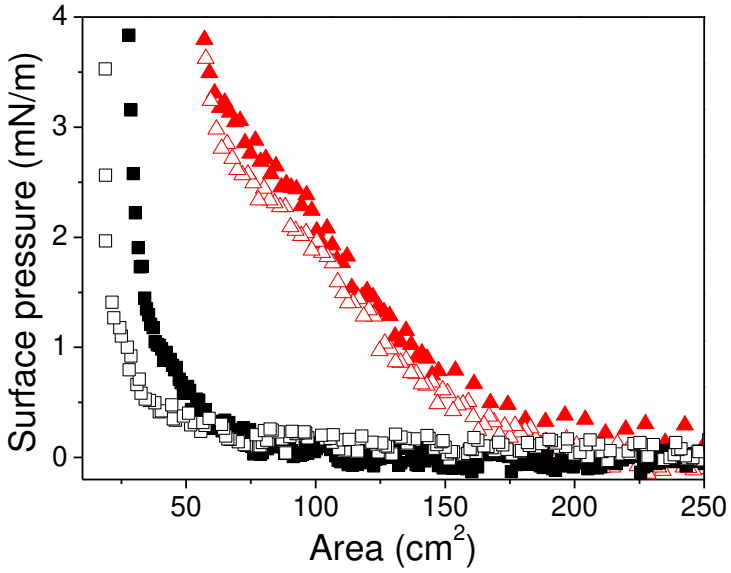


**Figure 4.** a) Consecutive compression isotherms for CPs8- (black symbols) and CPs40-laden (red symbols) interfaces. The closed and open symbols represent the first and second compressions, respectively.

**3.3 Interfacial rheology.** The shear rheology (elastic (*G'*) and viscous (*G"*) contributions) of CPs-laden interfaces under compression were studied using the ISR needle rheometer. The measurements were made under constant surface pressure by selecting the pressure control mode of the Langmuir trough once the target surface pressure had been attained. The magnetic needle of the shear rheometer was oscillated at an amplitude within the linear viscoelastic region and at a constant frequency, $F$ = 0.5 Hz (3.14 rad/s).[7]

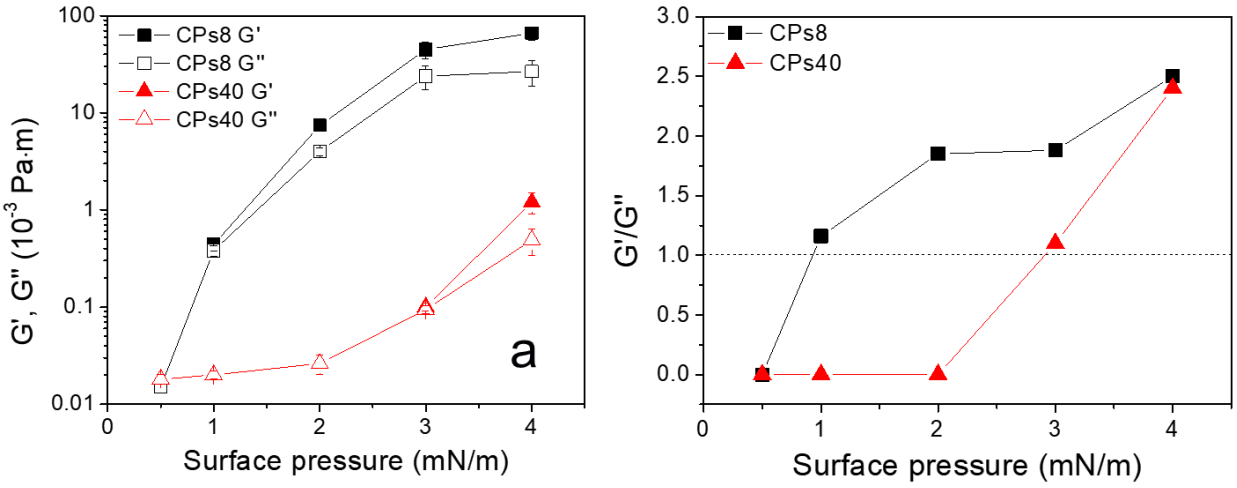


**Figure 5.** a) Dynamic surface shear moduli and b) the *G'/G''* ratio of CPs-laden interfaces as a function of increasing surface pressure.

The dynamic surface shear moduli of CPs8- and CPs40-laden interfaces with increasing surface pressure are compared in Fig. 5a. At 0.5 mN/m, both CPs8- and CPs40-laden interfaces are purely viscous (G" > G' = 0), with the liquid-like response confirming the particles to be readily mobile at the air-water interface. Both G' and G" increased with surface pressure, and a critical condition is reached when the particle-laden interfaces become solid-like (G' > G"), which was found at ~1 mN/m and ~ 3 mN/m for the CPs8- and CPs40-laden interfaces, respectively (Fig. 5b). Furthermore, those surface pressures correspond to the compressional L-S transition for both systems (Fig. 1). As shown in Fig. 5b, when in the S-phase ($\Pi$ = 4 mN/m), the ratios of G'/G" are equivalent for both CPs-laden interfaces (G'/G" ~2.5), although the viscoelastic moduli of the CPs8-laden interface is approximately two orders of magnitude higher than the CPs40-laden

interface, signifying greater mobility of CPs40 when highly compressed. When compressed at $\Pi$ = 3 mN/m (comparable to the condition in Figs. 2 and 3), the G'/G" ratio for CPs40 is ~1.0, while for CPs8 the interfacial shear rheology is strongly elastically dominant, with G' ~$50\times10^{-3}$ Pa·m. This further supports the reduced mobility of CPs8 in the particle-laden film, and with a high viscous component, justifies the unrelaxed-state of the compressed CPs8-laden interface.

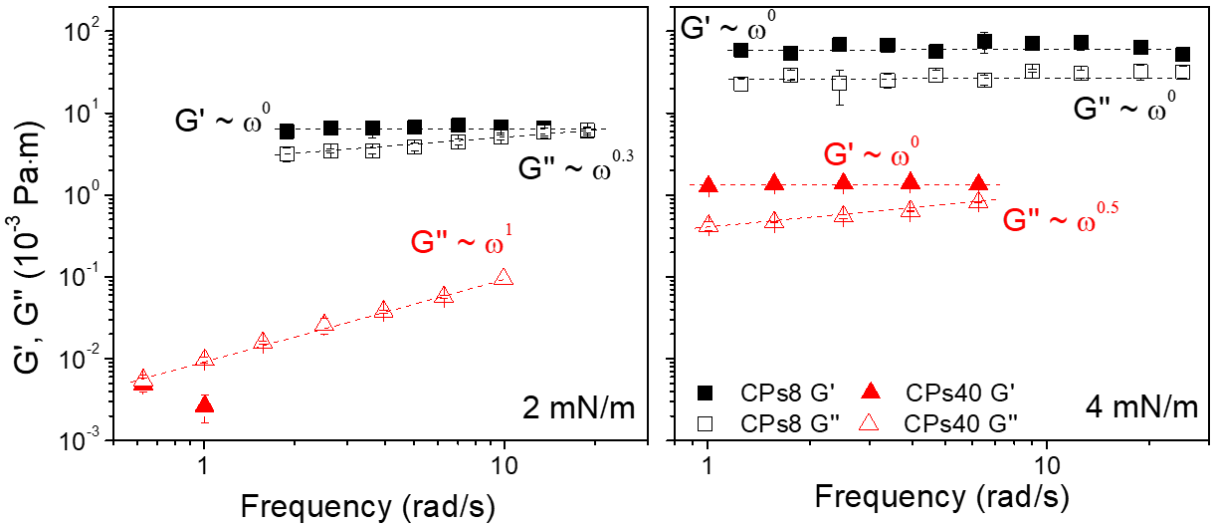


**Figure 6.** Frequency-dependent dynamic surface moduli of CPs-laden interfaces at $\Pi$ = 2 mN/m (a) and $\Pi$ = 4 mN/m (b). Black and red symbols correspond to the CPs8- and CPs40-laden interfaces, and open and closed symbols represent G' and G" values.

The time-dependent responses of CPs-laden interfaces were determined from frequency-sweeps performed in the linear viscoelastic regime.[7] Figure 6 shows the dynamic surface moduli measured as a function of oscillation frequency. At $\Pi$ = 0.5 mN/m, the responses of both CPs-laden interfaces were purely viscous (data not shown).[7] At $\Pi$ = 2mN/m (Fig. 6a), the CPs40-laden interface remained viscous-dominant, with G" ~ $\omega^{\sim 1}$, whereas G' was mostly unmeasurable over the frequency range as the phase difference between the stress and strain approached 90°.[7, 17] The G' response of the CPs8-laden interface was independent of frequency, confirming the onset of a glassy-state.[33] At $\Pi$ = 4 mN/m (Fig. 6b), the G' response of the CPs40-laden interface was also independent of frequency, and not unsurprising given that the particle-laden interface was

in the S-phase. The dependence of G" $\sim \omega^{\sim 0.5}$ suggests the mechanical response of the CPs40-laden interface is influenced by viscous forces,[34] i.e. likely the contribution from the polymer steric barrier. In comparison, both G' and G" of the CPs8-laden interface were found to be independent of frequency at $\Pi = 4\ mN/m$, confirming a glassy-state where the dynamics of the system are frozen.[29, 33]

For the ISR technique, the shear rheology is measured in the direction of uniaxial compression, with the oscillating needle positioned within an open-ended glass channel (Fig. S2). As such, with increasing compression and anisotropy of the particle-laden film (through wrinkle formation), only the shear component normal to the direction of compression is measured. While several studies measure surface pressure normal and parallel to the direction of compression, thus elucidating the surface pressure contributions from dilatational and shear deformations,[35, 36] to the authors knowledge there is no prior research measuring the directional shear rheology in compression. The research of Fuller and Vermant and co-workers have led developments in this field, and beyond the ISR technique, the study by Vermant using a modified double-wall ring (DWR) geometry with rotational rheometry is one other study that measured the interfacial shear rheology as a function of surface pressure controlled by a Langmuir trough compression.[23, 37, 38] Using a similar approach, Pepicelli et al. modified the DWR setup to study the shear rheology in pure compression with a radial trough.[39] The approach allowed the authors to distinguish between interfacial viscoelasticity induced by compression and those induced by the transient response of the network.

**Implications for foams:** When a foam is created there is often an excess of air-water surface area void of any stabilizing particles. This leads to bubble coalescence to reduce the total foam surface area until the interfaces of bubbles become 'jammed' by the particle network. Ceasing or reducing the coalescence rate occurs if particles are strongly irreversibly adsorbed at the air-water interface.[15] Previous studies have shown that bubble stability to coalescence is linked to the shear rheology, with interfacial films becoming resistant to yielding (a criteria needed for coalescence) when the G' contribution exceeds G".[6] The compressional data confirms that both CPs are interfacially active, and the build-up of surface pressure in compression confirms they are not easily displaced from the interface, due to the anchoring effect of the extended polymer shell.

A previous study indicated that for bubble stabilization to occur, the particle network should be compressed to the L-S transition.[7] For CPs8 and CPs40 this condition is at $\Pi$ ~1 mN/m and ~3 mN/m, respectively, and corresponds to the initial condition when the shear component G' exceeds G". At this critical condition, the G' value for CPs8 exceeds that of CPs40, which would correspond to a higher interfacial yield stress, hence the CPs8-stabilized foam should exhibit greater stability. Furthermore, bubble coarsening is often correlated to the compressional elasticity, with coarsening inhibited when $E > \frac{\gamma}{2}$, where E is the compressional elasticity and $\gamma$ the surface tension.[6] At the L-S transition, $E$ is ~10 mN/m for both CPs8 and CPs40, hence the effect of particle type on bubble (foam) coarsening is likely to be negligible.

Both CPs8 and CPs40 were used to stabilize foams and showed almost equivalent foamability but measurable differences in the foam stability, see Fig. 7a. Using CPs40, the initial rate of foam collapse was 2.1 cm/h, with the foam almost completely diminished within 1 h. For CPs8, the initial rate of foam collapse was 0.6 cm/h, with 50% and 33% of the foam remaining after 1 h and 2 h of aging. With bubble coarsening considered to be negligible but also found to occur over longer timescales,[15] the differences in foam stability were attributed to the resistance to bubble coalescence. When sampling the foams to measure the bubble size distribution (Fig. 7b), the CPs40 foam could not be transferred into the capillary cell without collapsing the foam, suggesting the foam is highly shear sensitive, which is attributed to the low interfacial shear viscoelasticity and high mobility of the CPs40 particles at the air-water interface. Transfer of the CPs8 foam to the capillary cell was achieved, and the mean bubble size at 5 and 60 min was 189 ± 69 and 465 ± 121 μm, signifying that bubble growth through coalescence governs the foam stability. The foam stability data is in good agreement with those observations made by studying the structure and shear rheology of a 2D-planar interface. At the condition when interfacial shear rheology strongly contributes to the bubble coalescence time (i.e. G' = G"), the viscoelastic moduli of the CPs8-laden interface is ~4 times that of the CPs40-laden interface, with this difference predominantly governing the rate of foam collapse.

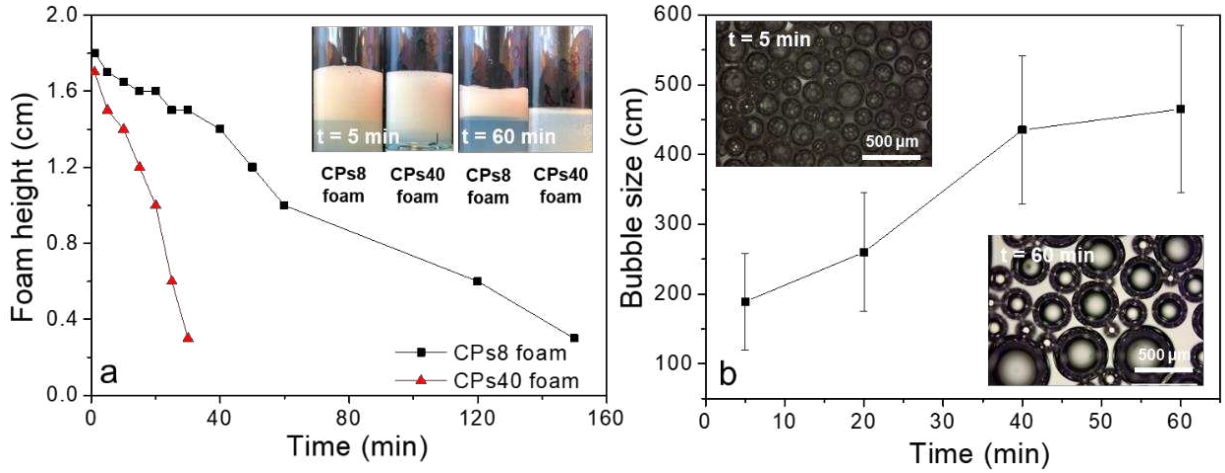


**Figure 7.** a) Stability of CPs8 and CPs40 foams (lines added to guide the eye). The inset images show the heights of each foam after 5 and 60 min of aging without disturbance. b) Bubble size distribution of the CPs8 foam, measured by sampling the foam and viewing the foam under 40× magnification optical microscope. Inset images of the CPs8 foam at 5 and 60 min after foam preparation and sampling.

## 4. CONCLUSION

Core-shell composite nanoparticles offer excellent foam stability by improving adsorption of nanoparticles at the air-water interface (contribution from the organic polymer), and by increasing the interfacial shear viscoelasticity (contributions from the inorganic particle and organic polymer). While most studies synthesize composite particles via chemical grafting methods,[8, 13, 24] few studies consider the foam stabilizing potential of composite nanoparticles formed by physical adsorption, a method that is more amenable to process scale-up.

Two CPs were prepared via a facile one-step physical adsorption method, forming core-shell nanocomposites with different polymer shell thicknesses. In compression, the CPs40-laden interface showed distinct gas-liquid-solid phase transitions and when reducing the surface pressure, the compressed particle-laden interface relaxed to its original state. The compressed-state of the CPs8-laden interface did not relax and wrinkles in the particle-laden film that had formed in compression remained due to greater adhesion between the compressed particles. It was shown

that 8 kDa PVP binds to silica to form a rigid film, unlike 40 kDa PVP that forms a more solvated film which exhibits greater viscoelasticity.[25] Such changes contributed to an apparent softening of particle-particle contacts that affected particle mobility in confinement.

In compression the shear viscoelasticity increased and the viscoelastic moduli (G' and G") were almost equivalent at the L-S phase transition, with the response being consistent for both CPs8 and CPs40-laden interfaces and previous findings.[7] However, the viscoelasticity was higher in the CPs8-laden interface compared to CPs40, with the rigidity partly a result of higher adhesion between 8 kDa PVP surfaces when compressed and held in contact for prolonged times. The reduced particle mobility in the CPs8-laden interface led to improved foam stability with the bubble coalescence rate retarded relative to the CPs40-laden interface.

This study has demonstrated a simple and effective method of modulating the interfacial film mechanical response, with the findings important to control the performance of foams, for example from EOR foams where strongly-stable interfaces are needed to maintain foam stability under elevated pressures and temperatures,[40-42] to targeted drug delivery where foam collapse can be triggered to release the stabilizing particles that carry the drug payload.[43-45] This work contributes to the body of literature which considers methods to tune behavior of particle-laden interfaces. The interface strongly governs the bulk properties of foams and further work is directed at optimizing the structure of the inorganic-organic composite to elevate interfacial viscoelasticity so as to strongly inhibit droplet coalescence and coarsening. Through this, new opportunities to develop long-lifetime foams using minimal stabilizing species can be realized.

## ASSOCIATED CONTENT

### Supporting Information

TGA profiles for silica nanoparticles, PVP-only, CPs8 and CPs40 (Fig. S1); PVP surface coverage, hydrodynamic diameter and thickness of hydrated PVP shell of the composite particles (Table S1); Digital photo of the Interfacial Shear Rheometer (ISR400) combined with a KSV NIMA Langmuir

trough (Fig. S2a); Schematic of the magnetic needle and its movement at the interface (Fig. S2b); $\Pi - A$ isotherms of CPs-laden interfaces. The inset compares the surface elasticity ($E_0 = -\frac{d\Pi}{dlnA}$) of the CPs8 and CPs40-laden interfaces as a function of surface area. The stars indicate the trough areas at the collapse point, which are ~ 25.6 $cm^2$ and ~52.8 $cm^2$ for the CPs8 and CPs40-laden interfaces respectively (Fig. S3); Adhesion force between PVP-PVP surfaces as a function of surface delay time measured via the AFM colloid probe technique (Fig. S4).

**Corresponding Author**

K.Y. – Email: victoryu66@ujs.edu.cn;

D. H. – Email: d.harbottle@leeds.ac.uk

**ACKNOWLEDGMENTS**

K.Y. would like to thank the Natural Science Foundation of Jiangsu Province (No. BK20210759), China Postdoctoral Science Foundation (No. 2020M681506), Senior Talent Foundation of Jiangsu University (19JDG029), and the Opening Fund of State Key Laboratory of Heavy Oil Processing (SKLOP202001001) for supporting this research. The authors would also like to acknowledge Prof. Zhenghe Xu (University of Alberta, Canada) who provided access to the ISR, and the experimental assistance of Mrs. Ni Yang (NINT, University of Alberta, Canada) who provided guidance on using the ISR.

## References

[1] F. Grillo, M.A. Fernandez-Rodriguez, M.N. Antonopoulou, D. Gerber, L. Isa, Nature 582 (2020) 219.

[2] A. Rauh, M. Rey, L. Barbera, M. Zanini, M. Karg, L. Isa, Soft Matter 13 (2017) 158.

[3] Y. Liu, B.P. Binks, J Colloid Interf Sci 583 (2021) 522.

[4] B. Robin, C. Albert, M. Beladjine, F.X. Legrand, S. Geiger, L. Moine, V. Nicolas, A. Canette, M. Trichet, N. Tsapis, F. Agnely, N. Huang, J Colloid Interf Sci 595 (2021) 202.

[5] Y. Liu, B.P. Binks, J Colloid Interf Sci 594 (2021) 204.

[6] K. Yu, B. Li, H.G. Zhang, Z.T. Wang, W. Zhang, D.B. Wang, H.J. Xu, D. Harbottle, J.F. Wang, J.M. Pan, Chem Eng J 416 (2021).

[7] K. Yu, H.G. Zhang, S. Biggs, Z.H. Xu, O.J. Cayre, D. Harbottle, J Colloid Interf Sci 527 (2018) 346.

[8] M. Rey, M.A. Fernandez-Rodriguez, M. Steinacher, L. Scheidegger, K. Geisel, W. Richtering, T.M. Squires, L. Isa, Soft Matter 12 (2016) 3545.
[9] J. Zhao, F. Torabi, J. Yang, Fuel 287 (2021) 119443.
[10] M. Rey, M.A. Fernandez-Rodriguez, M. Karg, L. Isa, N. Vogel, Accounts Chem Res 53 (2020) 414.
[11] M. Karg, A. Pich, T. Hellweg, T. Hoare, L.A. Lyon, J.J. Crassous, D. Suzuki, R.A. Gumerov, S. Schneider, I.I. Potemkin, W. Richtering, Langmuir 35 (2019) 6231.
[12] X.W. Gu, X.C. Ye, D.M. Koshy, S. Vachhani, P. Hosemann, A.P. Alivisatos, P Natl Acad Sci USA 114 (2017) 2836.
[13] X.C. Ye, C.H. Zhu, P. Ercius, S.N. Raja, B. He, M.R. Jones, M.R. Hauwiller, Y. Liu, T. Xu, A.P. Alivisatos, Nat Commun 6 (2015).
[14] K. Schwenke, L. Isa, D.L. Cheung, E. Del Gado, Langmuir 30 (2014) 12578.
[15] K. Yu, H. Zhang, C. Hodges, S. Biggs, Z. Xu, O.J. Cayre, D. Harbottle, Langmuir 33 (2017) 6528.
[16] J.S.J. Tang, R.S. Bader, E.S.A. Goerlitzer, J.F. Wendisch, G.R. Bourret, M. Rey, N. Vogel, Acs Omega 3 (2018) 12089.
[17] C.F. Brooks, G.G. Fuller, C.W. Frank, C.R. Robertson, Langmuir 15 (1999) 2450.
[18] M. Tanaka, S. Schiefer, C. Gege, R.R. Schmidt, G.G. Fuller, J Phys Chem B 108 (2004) 3211.
[19] P. Cicuta, E.J. Stancik, G.G. Fuller, Phys Rev Lett 90 (2003).
[20] C.A. Naumann, C.F. Brooks, G.G. Fuller, W. Knoll, C.W. Frank, Langmuir 15 (1999) 7752.
[21] R.E. Kurtz, A. Lange, G.G. Fuller, Langmuir 22 (2006) 5321.
[22] P.J. Beltramo, M. Gupta, A. Alicke, I. Liascukiene, D.Z. Gunes, C.N. Baroud, J. Vermant, P Natl Acad Sci USA 114 (2017) 10373.
[23] N. Jaensson, J. Vermant, Curr Opin Colloid In 37 (2018) 136.
[24] S.Q. Liu, H.Y. Wang, P. Akcora, Macromol Chem Phys 219 (2018).
[25] K. Yu, C. Hodges, S. Biggs, O.J. Cayre, D. Harbottlte, Ind Eng Chem Res 57 (2018) 2131.
[26] K. Yu, B. Li, Z.T. Wang, W. Zhang, D.B. Wang, H.J. Xu, J.F. Wang, D. Harbottle, Ind Eng Chem Res 59 (2020) 7495.
[27] E. Pensini, D. Harbottle, F. Yang, P. Tchoukov, Z.F. Li, I. Kailey, J. Behles, J. Masliyah, Z.H. Xu, Energ Fuel 28 (2014) 6760.
[28] R. Xu, E. Dickinson, B.S. Murray, Langmuir 23 (2007) 5005.
[29] H. Zhang, K. Yu, O.J. Cayre, D. Harbottle, Langmuir 32 (2016) 13472.
[30] K. Geisel, A.A. Rudov, I.I. Potemkin, W. Richtering, Langmuir 31 (2015) 13145.
[31] T. Li, G. Brandani, D. Marenduzzo, P.S. Clegg, Phys Rev Lett 119 (2017).
[32] R. Gurney, A. Henry, R. Schach, A. Lindner, C. Creton, Langmuir 33 (2017) 1670.
[33] A. Maestro, O.S. Deshmukh, F. Mugele, D. Langevin, Langmuir 31 (2015) 6289.
[34] V. Trappe, D.A. Weitz, Phys Rev Lett 85 (2000) 449.
[35] A. Alicke, S. Simon, J. Sjoblom, J. Vermant, Langmuir 36 (2020) 14942.
[36] M. Pepicelli, T. Verwijlen, T.A. Tervoort, J. Vermant, Soft Matter 13 (2017) 5977.
[37] E. Hermans, J. Vermant, Soft Matter 10 (2014) 175.
[38] C.O. Klein, A. Theodoratou, P.A. Ruhs, U. Jonas, B. Loppinet, M. Wilhelm, P. Fischer, J. Vermant, D. Vlassopoulos, Rheol Acta 58 (2019) 29.
[39] M. Pepicelli, N. Jaensson, C. Tregouet, B. Schroyen, A. Alicke, T. Tervoort, C. Monteux, J. Vermant, J Rheol 63 (2019) 815.

[40] N. Yekeen, M.A. Manan, A.K. Idris, E. Padmanabhan, R. Junin, A.M. Samin, A.O. Gbadamosi, I. Oguamah, J Petrol Sci Eng 164 (2018) 43.
[41] N. Yekeen, E. Padmanabhan, A.K. Idris, J Ind Eng Chem 66 (2018) 45.
[42] Z.X. Xu, B.F. Li, H.Y. Zhao, L. He, Z.L. Liu, D.Q. Chen, H.Y. Yang, Z.M. Li, Acs Omega 5 (2020) 19092.
[43] V. Poulichet, V. Garbin, P Natl Acad Sci USA 112 (2015) 5932.
[44] A. Huerre, M. De Corato, V. Garbin, Nat Commun 9 (2018).
[45] A. Jamburidze, A. Huerre, D. Baresch, V. Poulichet, M. De Corato, V. Garbin, Langmuir 35 (2019) 10087.